Journal of Advanced Ceramics
2018, **7**(4): 343–351
https://doi.org/10.1007/s40145-018-0284-2
ISSN 2226-4108
CN 10-1154/TQ

Research Article

Microstructural evolution and performance of carbon fiber-toughened ZrB_2 ceramics with SiC or $ZrSi_2$ additive

Kaixuan GUI[a,*], Fangyu LIU[a], Gang WANG[a], Zhongjia HUANG[a], Ping HU[b]

[a]*School of Materials Science and Engineering, Anhui Polytechnic University, Wuhu 241000, China*
[b]*National Key Laboratory of Science and Technology on Advanced Composites in Special Environments, Harbin Institute of Technology, Harbin 150001, China*

Received: March 1, 2018; Revised: May 16, 2018; Accepted: May 30, 2018

Abstract: ZrB_2–SiC/$ZrSi_2$ ceramics containing 30 vol% carbon fiber (C_f) additive were fabricated by hot pressing at low temperature (1500 ℃) using submicron ZrB_2 powders, and their microstructural evolution and performance were investigated. The addition of SiC or $ZrSi_2$ significantly reduced the onset sintering temperature and enhanced the densification of ZrB_2. ZrB_2–$ZrSi_2$–C_f showed poor performance owing to the serious fiber degradation, while the fiber degradation was effectively inhibited in ZrB_2–SiC–C_f resulting in high fracture toughness, substantial fiber pull-out, and non-brittle fracture mode for such material. The critical thermal shock temperature difference of ZrB_2–SiC–C_f was up to 741 ℃, significantly higher than those of ZrB_2–SiC/$ZrSi_2$ and ZrB_2–$ZrSi_2$–C_f. Moreover, this composite displayed a good oxidation resistance at 1500 ℃ in air.

Keywords: carbon fibers; microstructural evolution; hot pressing; thermal shock resistance; oxidation resistance

1 Introduction

Zirconium diboride (ZrB_2) is one of a family of transition metal boride compounds that belong to a class of materials known as ultra-high temperature ceramics (UHTCs). The combination of properties, such as high melting temperature (3250 ℃), high hardness (23 GPa), and high elastic modulus (> 500 GPa), makes ZrB_2 a very attractive candidate for several applications that include hypersonic flight, scramjet and rocket propulsion, atmospheric re-entry, refractory crucibles, and plasma-arc electrodes [1,2]. However, the high-temperature applications of monolithic ZrB_2 are limited due to its inherent brittleness and poor thermal shock resistance. Thus, a variety of reinforcements, such as particles [3], graphite flakes [4], whiskers [5], and fibers [6–9], have been adopted to toughen ZrB_2 ceramics via different toughening mechanisms. Carbon fiber has been widely researched as a toughening material for the ZrB_2-based UHTCs due to its large aspect ratio and good high-temperature stability. Nevertheless, because the required densification temperature for conventional ZrB_2-based ceramics is generally above 2000 ℃, the key problem in the fabrication of carbon fiber-toughened ZrB_2-based ceramics is the fiber degradation caused by the reaction between carbon fibers and ceramic compositions at high sintering temperature. Therefore, it is necessary to reduce the sintering temperature of ZrB_2-based ceramics or to use pitch-based fibers which can withstand high temperature [10,11].

* Corresponding author.
E-mail: guikx@ahpu.edu.cn

The strategy typically adopted to reduce the sintering temperature of ZrB_2 is to introduce sintering additives and/or to refine the starting powders down to submicron or nanoscale. Many researches have shown that silicon carbide (SiC) is the most common additive for ZrB_2 because it can improve the sinterability, inhibit grain growth, and increase the oxidation resistance of ZrB_2 as well [12,13]. Researches also reveal that zirconium disilicide ($ZrSi_2$) can facilitate full densification of ZrB_2 at low temperatures by particle deformation and formation of a grain-boundary amorphous film during hot pressing [14,15]. Another effective way to reduce the sintering temperature of ZrB_2 is to use nanosized powders as starting material instead of microsized powders since the sintering activity of nanosized particles is dramatically higher than that of their microsized counterparts [16–18].

The purpose of the present study is to fabricate the carbon fiber-toughened ZrB_2-based ceramics at low temperature by the incorporation of $ZrSi_2$ or SiC additive along with submicron ZrB_2 powders. The effects of $ZrSi_2$ and SiC on the densification behavior, mechanical properties, thermal shock resistance, and oxidation resistance of ZrB_2–C_f composites were investigated.

2 Experimental

The starting powders used in this study were as following: ZrB_2 powders (purity > 97%, metals basis, impurity content (wt%): C 0.25, O 1.50, N 0.25, Fe 0.1, Hf 0.2, D_{50} = 200 nm, supplied by Beijing HWRK Chem Co., Ltd., China), SiC powders (purity > 98%, impurity content (wt%): O 1.20, D_{50} = 0.45 μm, supplied by Kaihua, China), and $ZrSi_2$ powders (purity > 98.5%, D_{50} = 0.50 μm, supplied by Beijing HWRK Chem Co., Ltd., China). The carbon fiber selected in the present study was T800 carbon fiber (Tokyo, Japan) with an average diameter of 5 μm. Powder mixtures consisted of ZrB_2–20 vol% SiC/$ZrSi_2$ and ZrB_2–20 vol% SiC/$ZrSi_2$–30 vol% C_f were ball milled for 8 h in a polyethylene bottle using WC balls and ethanol as the grinding media, and then dried in a rotary evaporator at a temperature of 70 ℃ in vacuum and a rotation speed of 35 rpm. Before ball milling, the carbon fibers were chopped into short fibers of about 2 mm in length, which could facilitate their uniform distribution in the ceramic matrix. Powders were heated to 1500 ℃ at a rate of 15 ℃/min, under a uniaxial pressure of 30 MPa, and then held at this temperature for 1 h. After hot pressing, the furnace was cooled at a rate of ~20 ℃/min to room temperature. The shrinkage curve of the sample was recorded by a dilatometer at a resolution of 0.005 mm, and the reported powder shrinkage data was obtained by subtracting the thermal expansion of the graphite punches from the original recorded shrinkage data.

Densities of the samples were measured by the Archimedes method with deionized water as the immersing medium. Relative density was calculated via dividing bulk density to theoretical density. Flexural strength was measured by 3-point bending tests on 3 mm × 4 mm × 36 mm bars with a span of 30 mm at a crosshead speed of 0.5 mm/min. Fracture toughness was evaluated using single-edge notched beam (SENB) on 2 mm × 4 mm × 22 mm bars with a 16 mm span and a crosshead speed of 0.05 mm/min [19,20]. The reported averages and standard deviations of flexural strength and fracture toughness were calculated from a minimum of six bars. Microstructures were analyzed by scanning electron microscopy (SEM, FEI Sirion, the Netherlands) with energy dispersion spectroscopy (EDS).

The thermal shock behaviors of ZrB_2–SiC/$ZrSi_2$ and ZrB_2–SiC/$ZrSi_2$–C_f were evaluated by a water-quenching technique. The test bars were heated up to the testing temperatures from 200 to 800 ℃ in resistance heating furnace and held at a chosen temperature for 10 min to induce the homogeneous temperature distribution within them. The specimens were then subjected to a thermal shock by quenching them into a water bath from the preset temperatures. The residual flexural strengths of the specimens after quenching were measured by 3-point bending test. The critical thermal shock temperature difference (ΔT_c) of the composite was defined as the temperature difference at which the composite remained 70% of the room temperature strength, which was determined using linear interpolation of the residual strength values [21]. The oxidation of the ZrB_2–SiC/$ZrSi_2$–C_f composites was conducted at 1500 ℃ for 1 h in an electrical furnace in stagnant air using 3 mm × 4 mm × 36 mm test bars and the heating rate was 10 ℃/min. The microstructures of the surfaces and cross-sections of the composites after oxidation were analyzed by SEM.

3 Results and discussion

Typical SEM images of the starting ZrB_2 powders and the mixed ZrB_2–SiC–C_f powders are shown in Fig. 1

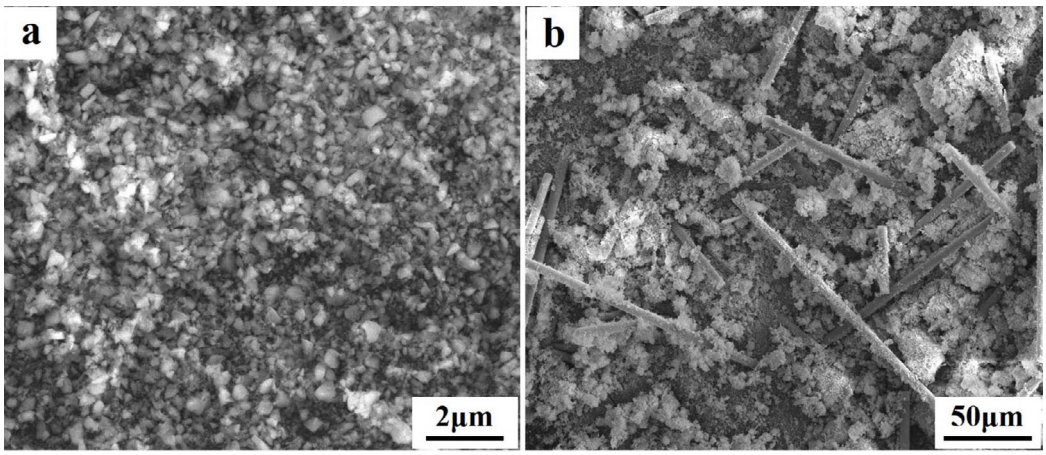

Fig. 1 SEM images of (a) the starting ZrB_2 powders and (b) the mixed ZrB_2–SiC–C_f powders.

revealing a uniform distribution of C_f in ZrB_2–SiC powders. To investigate the densification behaviors of ZrB_2, ZrB_2–SiC, and ZrB_2–$ZrSi_2$ ceramics with submicron ZrB_2 powders, typical densification curves of these materials by hot pressing at 1500 ℃ for 1 h are presented in Fig. 2 (inset is the heating curve). The onset densification temperature of submicron ZrB_2 powders is 1470 ℃, significantly lower than the typical value of 1700 ℃ for micro-sized ZrB_2 powders [22]. The decrease in onset densification temperature is attributed to the reduced particle size of the raw ZrB_2 powders from micro-scale to submicron-scale, which is believed to be an effective way to enhance the sinterability of ZrB_2-based ceramics [18]. Meanwhile, the onset densification temperatures of ZrB_2–SiC and ZrB_2–$ZrSi_2$ are obviously lower than that of monolithic ZrB_2, indicating that the addition of SiC or $ZrSi_2$ enhances the densification of submicron ZrB_2 powders. From the densification rate point of view, it seems that ZrB_2–SiC not only has a higher densification rate but also has a longer densification time than monolithic ZrB_2 during the initial stage of sintering, which leads to a higher relative density of ZrB_2–SiC (95.4%) compared with monolithic ZrB_2 (88.1%). For ZrB_2–$ZrSi_2$, rapid densification occurs at 1340 ℃ for 10 min and then markedly slows down until full densification achieves (99.9%). The results imply that $ZrSi_2$ is an effective sintering additive facilitating the full densification of ZrB_2-based ceramics at low temperatures. The high relative density of ZrB_2–$ZrSi_2$ ceramic results in obviously higher mechanical properties of such material compared to ZrB_2 and ZrB_2–SiC ceramics, as shown in Table 1.

Figure 3 shows the typical fracture surfaces of ZrB_2, ZrB_2–SiC, and ZrB_2–$ZrSi_2$ ceramics by hot pressing at 1500 ℃. Some pores are apparent in the micrographs of monolithic ZrB_2 (Fig. 3(a)), which is in accordance with the relatively low density of this material. Majority of these pores are located at ZrB_2 grain boundaries and others are trapped into ZrB_2 grains resulting in the intragranular pores. A significantly denser microstructure is obtained for ZrB_2–SiC (Fig. 3(b)) compared with that of monolithic ZrB_2 as the addition of SiC particles could improve the densification of ZrB_2-based ceramics. SiC grains with the dark contrast are mainly located at ZrB_2 grain boundaries or at multiple ZrB_2 grain junctions, which could act as grain growth inhibitors during hot pressing [23]. However, it seems that

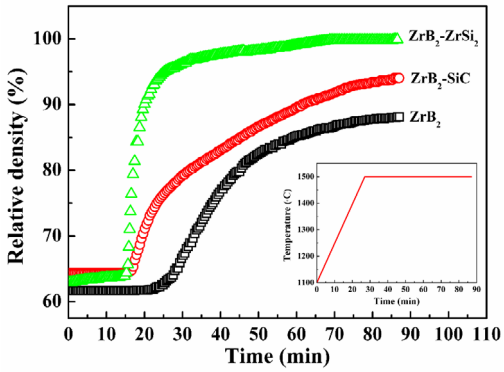

Fig. 2 Typical densification curves of ZrB_2, ZrB_2–SiC, and ZrB_2–$ZrSi_2$ ceramics by hot pressing at 1500 ℃ for 1 h.

Table 1 Relative densities and mechanical properties of investigated ZrB_2-based ceramics

Material	Relative density (%)	Flexural strength (MPa)	Fracture toughness (MPa·m$^{1/2}$)
ZrB_2	88.1	397±32	3.62±0.09
ZrB_2–SiC	95.4	592±69	5.34±0.12
ZrB_2–$ZrSi_2$	99.9	687±78	5.89±0.15
ZrB_2–SiC–C_f	95.0	335±18	6.05±0.14
ZrB_2–$ZrSi_2$–C_f	99.6	402±19	4.98±0.11

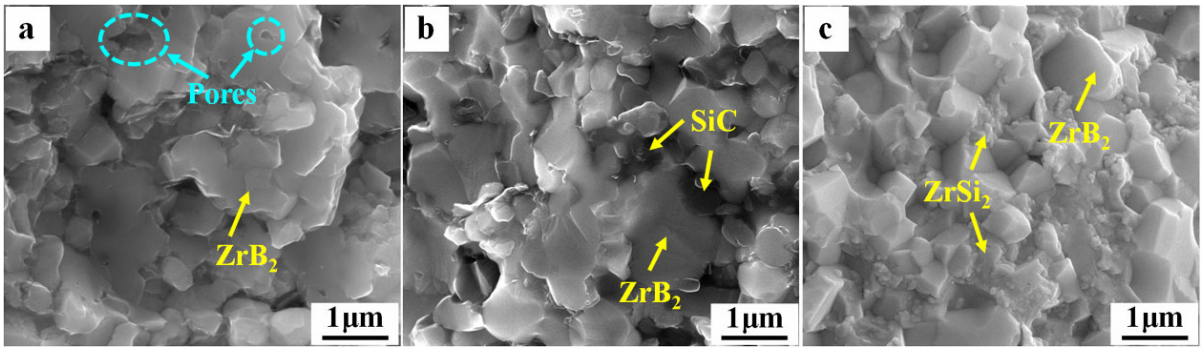

Fig. 3 SEM images of fracture surfaces of hot-pressed ceramics: (a) ZrB_2, (b) ZrB_2–SiC, and (c) ZrB_2–$ZrSi_2$.

ZrB_2–SiC has a larger grain size than monolithic ZrB_2. Researches on the sintering of many different materials have shown that grain growth is limited in very porous compacts when relative density is less than 90%, while rapid grain growth occurs in less porous solids when relative density is greater than 90% [24]. The relative densities of ZrB_2 and ZrB_2–SiC by hot pressing at 1500 ℃ for 1 h are 88.1% and 95.4%, respectively, which should be responsible for the difference in the grain sizes of ZrB_2 and ZrB_2–SiC. In the case of ZrB_2–$ZrSi_2$ ceramic, fully dense microstructure is achieved after sintering (Fig. 3(c)). The mud-like $ZrSi_2$ phase is distributed uniformly among ZrB_2 grains, which is believed to facilitate the particle rearrangement and thus enhanced densification during sintering.

Above results indicate that submicron ZrB_2 powders with addition of SiC or $ZrSi_2$ could be densified to high relative density at low temperature, which provides a promising way to fabricate carbon fiber-toughened ZrB_2-based ceramics with inhibited degradation of carbon fibers. In the present study, ZrB_2–C_f composites with SiC or $ZrSi_2$ addition were consolidated by hot pressing at 1500 ℃ for 1 h. Figure 4 reveals the fractured and polished surfaces of ZrB_2–$ZrSi_2$–C_f composite. The carbon fibers with an average length of ~100 μm, significantly shorter than the original length (~2 mm), are uniformly distributed in the ceramic matrix (Fig. 4(d)). The reduction in fiber length results

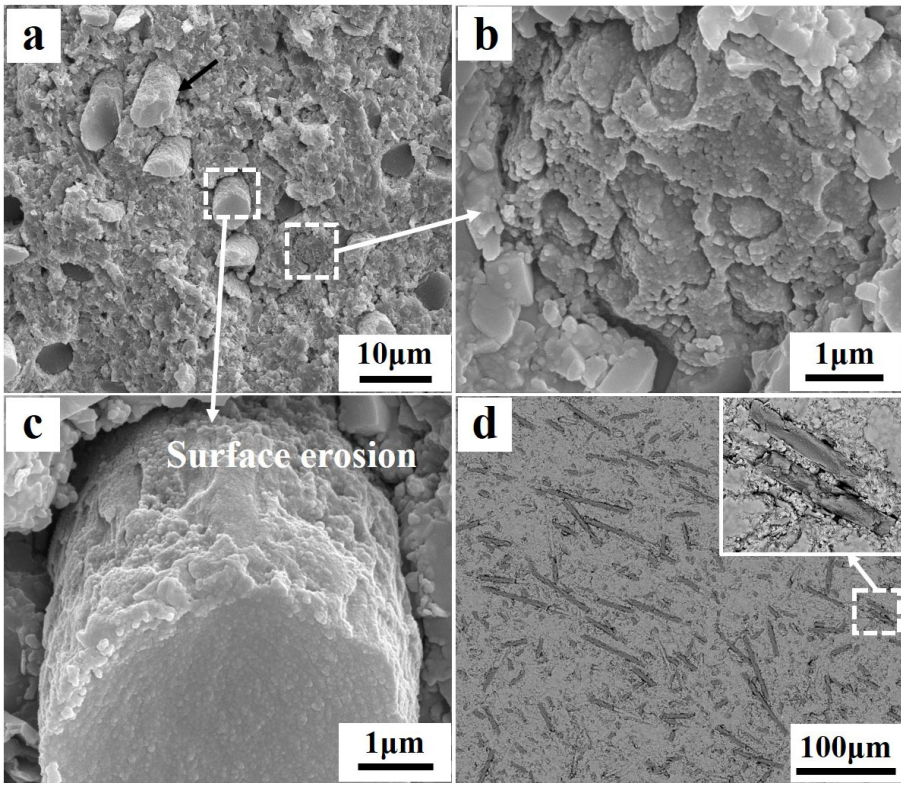

Fig. 4 SEM images of (a–c) fracture surface and (d) polished surface of ZrB_2–$ZrSi_2$–C_f composite.

from both the colliding of WC balls during ball milling and the applied pressure during sintering [25]. No obvious pores are detected on the polished surface of the ZrB_2–$ZrSi_2$–C_f composite, which is in accordance with its high relative density (99.6%). However, it should be noted that severe fiber erosions are observed from Figs. 4(a)–4(c) implying that the addition of $ZrSi_2$ causes the degradation of carbon fibers during sintering, which leads to the limited fiber pull-out and thus weakens the toughening effect of carbon fibers in the ZrB_2–$ZrSi_2$–C_f composite. It is believed that $ZrSi_2$ is not stable under vacuum condition at temperatures over 1400 ℃ and a possible reaction between carbon fibers and $ZrSi_2$ is as following [26]:

$$ZrSi_2 + 3C \rightarrow 2SiC + ZrC \quad (1)$$

The XRD pattern of the ZrB_2–$ZrSi_2$–C_f composite hot pressed at 1500 ℃ is shown in Fig. 5, in which some ZrC and SiC peaks are detected. The results indicate that the reaction between $ZrSi_2$ and C_f really occurs.

However, ZrB_2–SiC–C_f composite shows an obviously different microstructural evolution compared

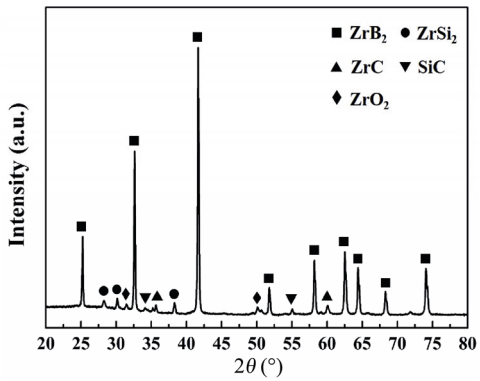

Fig. 5 XRD pattern of the ZrB_2–$ZrSi_2$–C_f composite hot pressed at 1500 ℃.

to ZrB_2–$ZrSi_2$–C_f, as shown in Fig. 6. Likewise, the carbon fibers with an average length of ~100 μm are uniformly distributed in the ceramic matrix (Fig. 6(a)), while the degradation of carbon fibers in ZrB_2–SiC–C_f is effectively inhibited at 1500 ℃. Fiber pull-out is clearly observed on the fracture surface of ZrB_2–SiC–C_f with a significant longer pull-out length than that of ZrB_2–$ZrSi_2$–C_f, which should be mainly due to the different strengths of carbon fibers in these two composites after sintering. Fiber erosions caused by the reaction between carbon fibers and $ZrSi_2$ in ZrB_2–$ZrSi_2$–C_f (Fig. 4) would reduce the strength of the carbon fiber, which in turn results in a short pull-out length. In contrast, the carbon fiber in ZrB_2–SiC–C_f has a smooth surface and a dense microstructure (Fig. 6(b)) implying that the fiber degradation is effectively inhibited during sintering. So it has sufficient strength to bear the interfacial shear during pulling out leading to a longer pull-out length. In addition, research has shown that an extensive fiber pull-out indicates a relatively weak fiber/matrix interfacial bonding, while a flat fracture surface indicates a strong fiber/matrix interfacial bonding [27]. The substantial fiber pull-out in ZrB_2–SiC–C_f implies a moderate ceramic/fiber interface bonding in this composite.

The flexural strength and fracture toughness of ZrB_2–$ZrSi_2$–C_f and ZrB_2–SiC–C_f composites are summarized in Table 1. Due to the lower relative density of ZrB_2–SiC–C_f, the flexural strength of such material is only 335±18 MPa, lower than that of ZrB_2–$ZrSi_2$–C_f composite (402±19 MPa). However, the fracture toughness of ZrB_2–SiC–C_f achieves as high as 6.05±0.14 MPa·$m^{1/2}$, much higher than that of ZrB_2–$ZrSi_2$–C_f composite (4.98±0.11 MPa·$m^{1/2}$). The remarkable improvement in

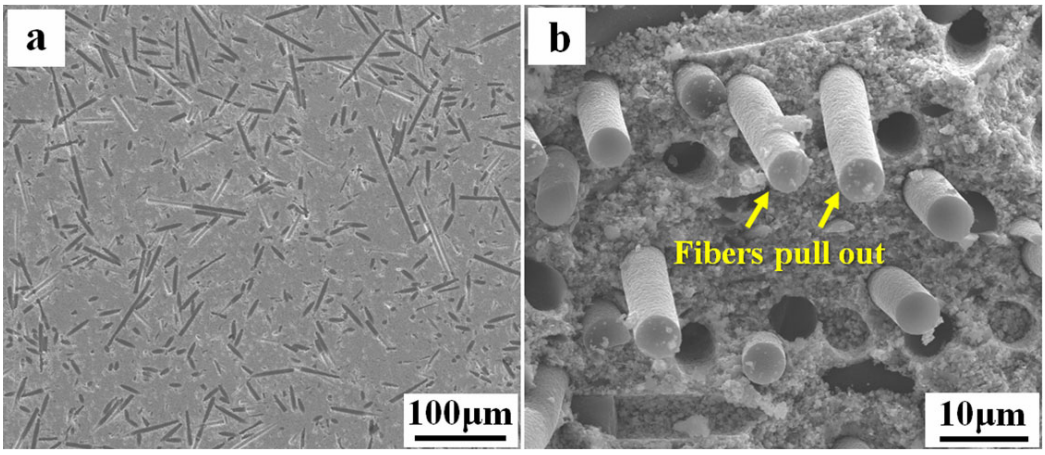

Fig. 6 SEM images of (a) polished surface and (b) fracture surface of ZrB_2–SiC–C_f composite.

fracture toughness for ZrB_2–SiC–C_f is principally attributed to the substantial fiber pull-out. It can be concluded that the flexural strength of the carbon fiber-toughened ZrB_2-based ceramic is strongly depended on its relative density, while the fracture toughness is mainly determined by the toughening effect of carbon fibers. To investigate fracture modes of ZrB_2–$ZrSi_2$–C_f and ZrB_2–SiC–C_f composites, their flexural stress–strain responses are displayed in Fig. 7. ZrB_2–$ZrSi_2$–C_f shows a typical brittle fracture mode although substantial volume fraction (30 vol%) of carbon fibers has been introduced in the composite, which should be ascribed to the severe degradation of carbon fibers. Despite having a lower flexural strength, ZrB_2–SiC–C_f shows a higher damage tolerance (defined as the flexural strain at which the flexural strength reaches maximum value) and a lower elastic modulus (evaluated as the slope of the flexural stress–strain curve before fracture) compared to ZrB_2–$ZrSi_2$–C_f composite. The thermal stress fracture resistance parameter, R, expressed by Eqs. (2) and (3), is often used to evaluate the thermal shock stress crack initiation and propagation behavior of ceramics [28]:

$$R = \frac{\sigma(1-\upsilon)}{E\alpha} \tag{2}$$

$$R' = \frac{\sigma(1-\upsilon)\lambda}{E\alpha} \tag{3}$$

where σ is the tensile strength, E is the Young's modulus, λ is the thermal conductivity, α is the coefficient of thermal expansion, and υ is the Poisson's ratio. Higher R and R' represent greater resistance to the initiation of fracture during rapid quenching and during steady-state heat flow down at a steep temperature gradient. Therefore, the lower elastic modulus is benefit to improve the thermal shock resistance of the ZrB_2–SiC–C_f composite, as discussed in the following section. Moreover, the ZrB_2–SiC–C_f composite exhibits a non-brittle fracture mode, indicating that ZrB_2–SiC–C_f composite has a higher damage tolerance. This should be attributed to the inhibited degradation of carbon fibers in ZrB_2–SiC–C_f during sintering which could facilitate some toughening mechanisms during fracture of this material, especially for fiber pull-out.

The thermal shock resistances of ZrB_2–SiC, ZrB_2–$ZrSi_2$, ZrB_2–SiC–C_f, and ZrB_2–$ZrSi_2$–C_f were evaluated by water-quenching technique, and the residual strength (σ_R) vs. temperature difference (ΔT) curves of these materials are shown in Fig. 8. The calculated critical

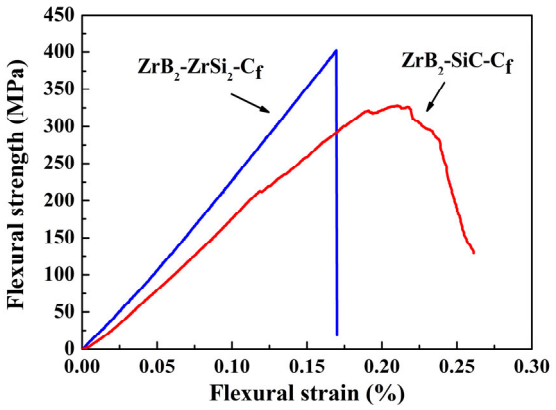

Fig. 7 Flexural strength–strain response of ZrB_2–$ZrSi_2$–C_f and ZrB_2–SiC–C_f composites.

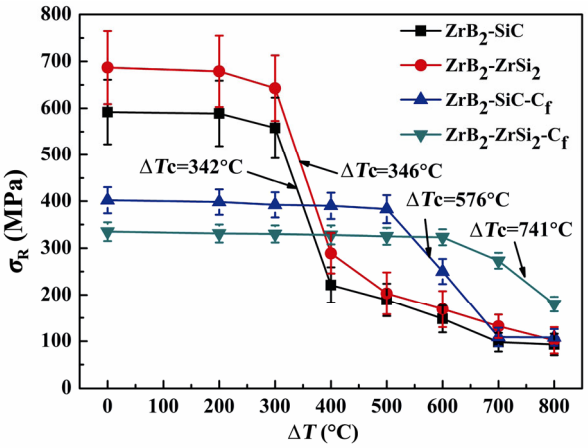

Fig. 8 Residual strength vs. thermal shock temperature difference for ZrB_2–SiC, ZrB_2–$ZrSi_2$, ZrB_2–SiC–C_f, and ZrB_2–$ZrSi_2$–C_f composites.

thermal shock temperature differences (ΔT_c) of ZrB_2–SiC and ZrB_2–$ZrSi_2$ are 342 and 346 ℃, respectively, obviously lower than those of ZrB_2–SiC–C_f and ZrB_2–$ZrSi_2$–C_f, implying that the incorporation of carbon fibers into ZrB_2-based ceramics improves the thermal shock resistance of such materials. For ZrB_2–$ZrSi_2$–C_f, the residual strength is almost kept at the initial strength as ΔT increases up to 500 ℃, and then decreases remarkably with the further increase of ΔT. The calculated ΔT_c for ZrB_2–$ZrSi_2$–C_f is 576 ℃, higher than the reported values for ZrB_2-based ceramics (ΔT_c = 345–500 ℃) [29,30]. Our previous study has revealed that the microstructure of carbon fibers in the ZrB_2-based ceramics strongly affects the thermal shock resistance of such material, and the inhibited degradation of carbon fibers facilitates to improve the thermal shock resistance [31]. As expected, the residual strength of ZrB_2–SiC–C_f retains at initial strength even ΔT is increased to 600 ℃ and then

gradually reduces to 54% of the initial strength as ΔT is increased up to 800 ℃. The calculated ΔT_c for ZrB_2–SiC–C_f composite is as high as 741 ℃, significantly higher than that of the ZrB_2–$ZrSi_2$–C_f composite. The excellent thermal shock resistance of ZrB_2–SiC–C_f composite should mainly result from the effectively inhibited degradation of carbon fibers in such material during low-temperature hot pressing, which provides significance for fabrication of ZrB_2-based ultra-high temperature ceramics with high reliability.

To investigate the oxidation behaviors of the ZrB_2–$ZrSi_2$–C_f and ZrB_2–SiC–C_f composites, they were oxidized in stagnant air at 1500 ℃ for 1 h. The weights of ZrB_2–SiC–C_f before and after oxidation are 1.718 and 1.707 g, respectively. The weights of ZrB_2–$ZrSi_2$–C_f before and after oxidation are 1.953 and 1.940 g, respectively. The oxidation of carbon fibers located on the surfaces of these two composites should be responsible for the weight loss during oxidation. Dense SiO_2 layers (detected by EDS from the area analysis) generate on the surfaces of these two composites after oxidation as indicated in Figs. 9(a)

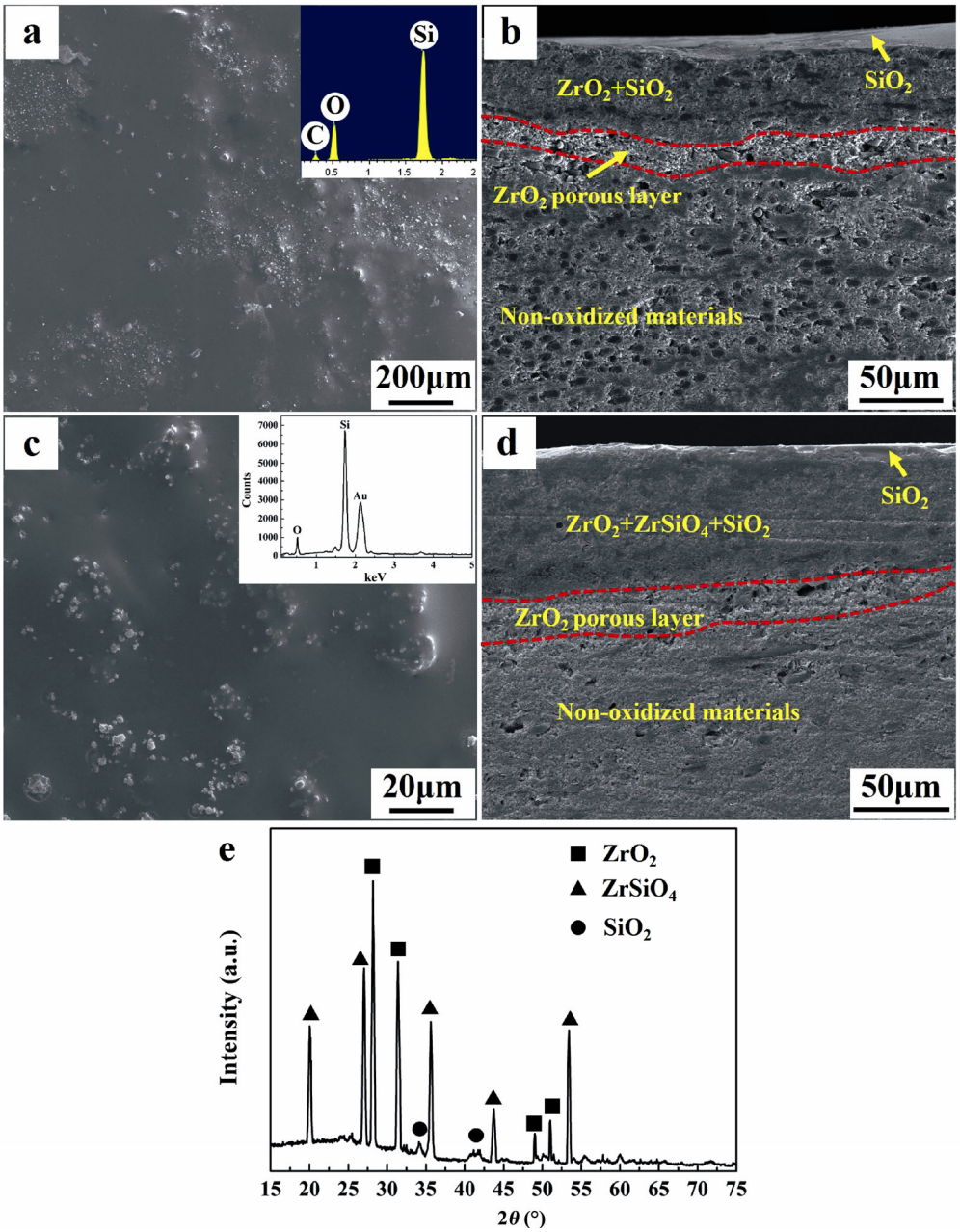

Fig. 9 SEM images of the surfaces and cross-sections of (a, b) ZrB_2–SiC–C_f and (c, d) ZrB_2–$ZrSi_2$–C_f composites oxidized in air at 1500 ℃ for 1 h, and (e) is the XRD pattern of the ZrO_2+$ZrSiO_4$+SiO_2 layer shown in (d).

and 9(c), which is believed to be an effective barrier for the diffusion of oxygen and thus protect the materials from further oxidation [32–34]. SEM images of the cross-sections show that the oxide scales with 50 and 90 μm in depth for ZrB_2–SiC–C_f and ZrB_2–$ZrSi_2$–C_f respectively are consisted of three layers, as shown in Figs. 9(b) and 9(d). For ZrB_2–SiC–C_f, a dense ZrO_2+SiO_2 layer is detected below the outmost SiO_2 layer and a porous ZrO_2 layer (i.e., SiC-depleted layer) generated between the ZrO_2+SiO_2 layer and the inner non- oxidized materials. In the case of ZrB_2–$ZrSi_2$–C_f, a similar layered structure of oxide scale is identified, which is composed of SiO_2 layer, ZrO_2+$ZrSiO_4$+SiO_2 layer (as identified by XRD shown in Fig. 9(e)), and the inner ZrO_2 porous layer. As the temperature elevates, ZrB_2 is preferentially oxidized producing ZrO_2 and B_2O_3. B_2O_3 is a liquid phase above 450 ℃ and it would volatilize at temperatures above 1100 ℃ resulting in porous ZrO_2 skeleton. At this temperature, the oxidation of $ZrSi_2$ has occurred and the resultant SiO_2 liquid phase flows from the site of oxidation (ZrO_2 porous layer) toward the surface of the material (SiO_2 layer) and fills the ZrO_2 skeleton near the surface of the material (ZrO_2+$ZrSiO_4$+SiO_2 layer). Studies have shown that the addition of SiC or $ZrSi_2$ can significantly improve the oxidation resistance of ZrB_2 ceramics, and our present study demonstrates that both the ZrB_2–SiC–C_f and ZrB_2–$ZrSi_2$–C_f composites exhibit good oxidation resistance, indicating that the introduction of 30 vol% carbon fibers into ZrB_2–SiC or ZrB_2–$ZrSi_2$ has minor effect on the oxidation resistance of these materials.

4 Conclusions

Microstructural evolution and mechanical properties of ZrB_2–SiC/$ZrSi_2$ ceramics containing 30 vol% C_f were investigated by hot pressing at 1500 ℃ using submicron ZrB_2 powders. ZrB_2 ceramics with and without SiC or $ZrSi_2$ additive showed distinctly different densification behaviors. The addition of SiC or $ZrSi_2$ significantly enhanced the densification of ZrB_2 and reduced the onset sintering temperature from 1470 to 1340 ℃, and ZrB_2–$ZrSi_2$ achieved full densification at 1500 ℃. However, serious fiber degradation occurred in ZrB_2–$ZrSi_2$–C_f composite by hot pressing at 1500 ℃, leading to low fracture toughness, limited fiber pull-out, and brittle fracture mode of such material. Fiber degradation was effectively inhibited when SiC was incorporated instead of $ZrSi_2$, and the ZrB_2–SiC–C_f composite exhibited a high fracture toughness (6.05±0.14 MPa·$m^{1/2}$), significant fiber pull-out, and a typical non-brittle fracture mode. The critical thermal shock temperature difference of ZrB_2–SiC–C_f was up to 741 ℃, remarkably higher than those of ZrB_2–SiC, ZrB_2–$ZrSi_2$, and ZrB_2–$ZrSi_2$–C_f, demonstrating an excellent thermal shock resistance of such composite. Meanwhile, both ZrB_2–SiC–C_f and ZrB_2–$ZrSi_2$–C_f composites exhibited good oxidation resistance at 1500 ℃ in air. This work offers great potential for fabrication of ZrB_2-based UHTCs with excellent properties.

Acknowledgements

Financial support was provided by Scientific Research Starting Foundation of Anhui Polytechnic University of China (No. 2017YQQ009) and the Fundamental Research Funds for the Central Universities (Grant No. HIT.BRETIII.201506).

References

[1] Fahrenholtz WG, Hilmas GE, Talmy IG, *et al*. Refractory diborides of zirconium and hafnium. *J Am Ceram Soc* 2007, **90**: 1347–1364.

[2] Guo S-Q. Densification of ZrB_2-based composites and their mechanical and physical properties: A review. *J Eur Ceram Soc* 2009, **29**: 995–1011.

[3] Monteverde F. Beneficial effects of an ultra-fine α-SiC incorporation on the sinterability and mechanical properties of ZrB_2. *Appl Phys A* 2006, **82**: 329–337.

[4] Zhi W, Zhanjun W, Guodong S. Fabrication, mechanical properties and thermal shock resistance of a ZrB_2-graphite ceramic. *Int J Refract Met H* 2011, **29**: 351–355.

[5] Silvestroni L, Sciti D, Melandri C, *et al*. Toughened ZrB_2-based ceramics through SiC whisker or SiC chopped fiber additions. *J Eur Ceram Soc* 2010, **30**: 2155–2164.

[6] Tang S, Hu C. Design, preparation and properties of carbon fiber reinforced ultra-high temperature ceramic composites for aerospace applications: A review. *J Mater Sci Technol* 2017, **33**: 117–130.

[7] Wang Y, Liu W, Cheng L, *et al*. Preparation and properties of 2D C/ZrB_2–SiC ultra high temperature ceramic composites. *Mat Sci Eng A* 2009, **524**: 129–133.

[8] Guo S. Hot-pressed laminated composites consisting of ZrB_2–SiC ceramic and C_f/ZrB_2–SiC composites. *J Ceram Soc Jpn* 2016, **124**: 166–171.

[9] Yang F, Zhang X, Han J, *et al*. Mechanical properties of short carbon fiber reinforced ZrB_2–SiC ceramic matrix composites. *Mater Lett* 2008, **62**: 2925–2927.

[10] Silvestroni L, Fabbriche DD, Melandri C, *et al*. Relationships between carbon fiber type and interfacial domain in ZrB_2-based ceramics. *J Eur Ceram Soc* 2016, **36**: 17–24.
[11] Zoli L, Vinci A, Silvestroni L, *et al*. Rapid spark plasma sintering to produce dense UHTCs reinforced with undamaged carbon fibres. *Mater Design* 2017, **130**: 1–7.
[12] Hwang SS, Vasiliev AL, Padture NP. Improved processing and oxidation-resistance of ZrB_2 ultra-high temperature ceramics containing SiC nanodispersoids. *Mat Sci Eng A* 2007, **464**: 216–224.
[13] Zhu S, Fahrenholtz WG, Hilmas GE. Influence of silicon carbide particle size on the microstructure and mechanical properties of zirconium diboride–silicon carbide ceramics. *J Eur Ceram Soc* 2007, **27**: 2077–2083.
[14] Wang M, Wang C-A, Zhang X. Effects of SiC platelet and $ZrSi_2$ additive on sintering and mechanical properties of ZrB_2-based ceramics by hot-pressing. *Mater Design* 2012, **34**: 293–297.
[15] Guo S, Nishimura T, Kagawa Y. Low-temperature hot pressing of ZrB_2-based ceramics with $ZrSi_2$ additives. *Int J Appl Ceram Tec* 2011, **8**: 1425–1435.
[16] Walker LS, Pinc WR, Corral EL. Powder processing effects on the rapid low-temperature densification of ZrB_2–SiC ultra-high temperature ceramic composites using spark plasma sintering. *J Am Ceram Soc* 2012, **95**: 194–203.
[17] Zamora V, Ortiz AL, Guiberteau F, *et al*. Spark-plasma sintering of ZrB_2 ultra-high-temperature ceramics at lower temperature via nanoscale crystal refinement. *J Am Ceram Soc* 2012, **32**: 2529–2536.
[18] Zamora V, Ortiz AL, Guiberteau F, *et al*. Crystal-size dependence of the spark-plasma-sintering kinetics of ZrB_2 ultra-high-temperature ceramics. *J Eur Ceram Soc* 2012, **32**: 271–276.
[19] Yang F, Zhang X, Han J, *et al*. Characterization of hot-pressed short carbon fiber reinforced ZrB_2–SiC ultra-high temperature ceramic composites. *J Alloys Compd* 2009, **472**: 395–399.
[20] Xiao K, Guo Q, Liu Z, *et al*. Influence of fiber coating thickness on microstructure and mechanical properties of carbon fiber-reinforced zirconium diboride based composites. *Ceram Int* 2014, **40**: 1539–1544.
[21] Zimmermann JW, Hilmas GE, Fahrenholtz WG. Thermal shock resistance of ZrB_2 and ZrB_2–30% SiC. *Mater Chem Phys* 2008, **112**: 140–145.
[22] Thompson M, Fahrenholtz WG, Hilmas G. Effect of starting particle size and oxygen content on densification of ZrB_2. *J Am Ceram Soc* 2011, **94**: 429–435.
[23] Guo W-M, Zhang G-J. Oxidation resistance and strength retention of ZrB_2–SiC ceramics. *J Eur Ceram Soc* 2010, **30**: 2387–2395.
[24] Wang H, Fang ZZ, Hwang KS. Kinetics of initial coarsening during sintering of nanosized powders. *Metall and Mat Trans A* 2011, **42**: 3534–3542.
[25] Sciti D, Zoli L, Silvestroni L, *et al*. Design, fabrication and high velocity oxy-fuel torch tests of a C_f–ZrB_2-fiber nozzle to evaluate its potential in rocket motors. *Mater Design* 2016, **109**: 709–717.
[26] Sha JJ, Li J, Wang SH, *et al*. Toughening effect of short carbon fibers in the ZrB_2–$ZrSi_2$ ceramic composites. *Mater Design* 2015, **75**: 160–165.
[27] He X, Guo Y, Zhou Y, *et al*. Microstructures of short-carbon-fiber-reinforced SiC composites prepared by hot-pressing. *Mater Charact* 2008, **59**: 1771–1775.
[28] Hasselman DPH. Strength behavior of polycrystalline alumina subjected to thermal shock. *J Am Ceram Soc* 1970, **53**: 490–495.
[29] Hu P, Gui K, Hong W, *et al*. High-performance ZrB_2–SiC–C_f composite prepared by low-temperature hot pressing using nanosized ZrB_2 powder. *J Eur Ceram Soc* 2017, **37**: 2317–2324.
[30] Sciti D, Silvestroni L, Saccone G, *et al*. Effect of different sintering aids on thermo-mechanical properties and oxidation of SiC fibers-reinforced ZrB_2 composites. *Mater Chem Phys* 2013, **137**: 834–842.
[31] Gui K, Hu P, Hong W, *et al*. Microstructure, mechanical properties and thermal shock resistance of ZrB_2–SiC–C_f composite with inhibited degradation of carbon fibers. *J Alloys Compd* 2017, **706**: 16–23.
[32] Zhang X-H, Hu P, Han J-C. Structure evolution of ZrB_2–SiC during the oxidation in air. *J Mater Res* 2008, **23**: 1961–1972.
[33] Rezaie A, Fahrenholtz WG, Hilmas GE. Evolution of structure during the oxidation of zirconium diboride-silicon carbide in air up to 1500 ℃. *J Eur Ceram Soc* 2007, **27**: 2495–2501.
[34] Vinci A, Zoli L, Landi E, *et al*. Oxidation behaviour of a continuous carbon fibre reinforced ZrB_2–SiC composite. *Corros Sci* 2017, **123**: 129–138.